Chem

Article

Identifying the lithium bond and lithium ionic bond in electrolytes

Graphical abstract

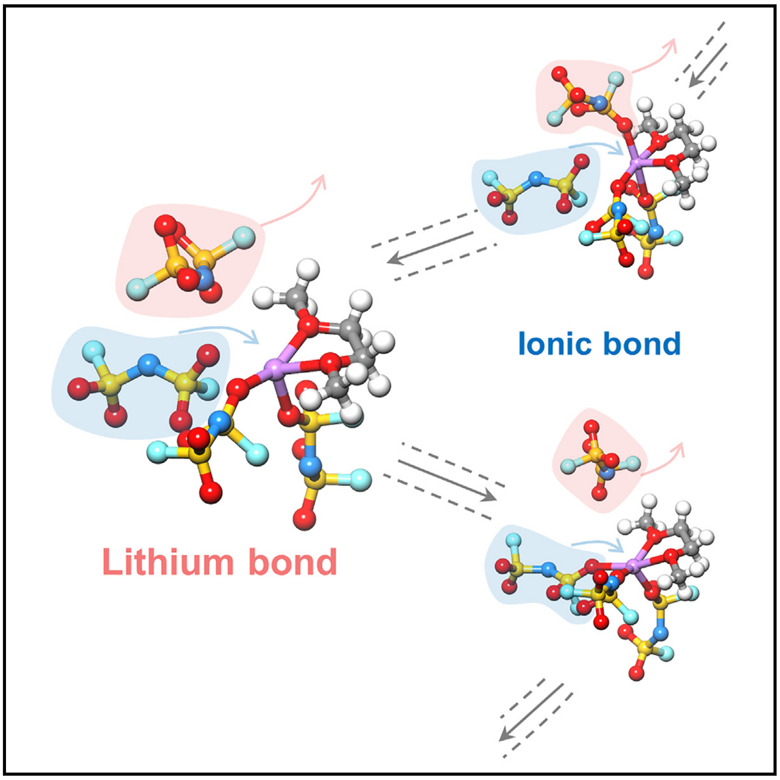

Highlights

- The Li bond and Li ionic bond in electrolytes are differentiated
- A coordination number of 4 is the critical point between the Li bond and ionic bond
- The Li bond is dominated by a strong electron localization effect

Authors

Nan Yao, Xiang Chen, Shu-Yu Sun, ..., Yan-Bin Gao, Wei-Lin Li, Qiang Zhang

Correspondence

xiangchen@mail.tsinghua.edu.cn (X.C.), zhang-qiang@mails.tsinghua.edu.cn (Q.Z.)

In brief

The bonding chemistry of lithium (Li) attracts great attention due to the widely applied Li batteries. Herein, we identified the Li bond and Li ionic bond according to the distinct variation trends of their chemical shifts in nuclear magnetic resonance spectroscopy. An electron localization effect and electrostatic interactions were found to dominate in these two bond types, respectively. Our work reveals the fundamental difference between the Li bond and the Li ionic bond, promoting the development of Li chemistry and related applications.

Yao et al., 2025, Chem *11*, 102254
January 9, 2025 © 2024 Elsevier Inc. All rights are reserved, including those for text and data mining, AI training, and similar technologies.
https://doi.org/10.1016/j.chempr.2024.07.016

CellPress

Chem

CellPress

Article

Identifying the lithium bond and lithium ionic bond in electrolytes

Nan Yao,[1] Xiang Chen,[1,*] Shu-Yu Sun,[1] Yu-Chen Gao,[1] Legeng Yu,[1] Yan-Bin Gao,[1] Wei-Lin Li,[1] and Qiang Zhang[1,2,*]

[1]Tsinghua Center for Green Chemical Engineering Electrification (CCEE), Beijing Key Laboratory of Green Chemical Reaction Engineering and Technology, Department of Chemical Engineering, Tsinghua University, Beijing 100084, China

[2]Lead contact

*Correspondence: xiangchen@mail.tsinghua.edu.cn (X.C.), zhang-qiang@mails.tsinghua.edu.cn (Q.Z.)

https://doi.org/10.1016/j.chempr.2024.07.016

THE BIGGER PICTURE Lithium (Li) has become one of the most well-known elements due to its wide applications in various fields, especially Li batteries. This leads to the intense research attention to Li chemistry and its bonding nature. Li shares the most authentic similarity with hydrogen (H) in the electronic structure among all the elements on the periodic table. The Li bond was therefore proposed as an analog of the H bond. However, the nature of the Li bond and the difference between the Li bond and Li ionic bond are far from clear.

Herein, we characterized the Li bonding chemistry in Li battery electrolytes by nuclear magnetic resonance spectroscopy. The Li bond and Li ionic bond were identified according to inverse ^{7}Li chemical shifts with increasing bond strength. An electron localization effect and electrostatic interactions were found to dominate in these two bond types. This work affords a clear identification of the Li bond and Li ionic bond, contributing to the development of Li chemistry.

SUMMARY

Lithium (Li) chemistry has been a significant branch of modern chemistry due to its wide and critical applications, such as Li batteries. Similar to the hydrogen (H) bond, the Li bond is the central topic of Li chemistry, but its nature is far from clear. Herein, the fundamental chemistry of the Li bond is systematically investigated, taking Li battery electrolytes as an example. Specifically, the Li bond and Li ionic bond can be differentiated according to nuclear magnetic resonance spectroscopy as ^{7}Li chemical shifts exhibit a downfield and upfield shift, respectively. The downfield shift indicates an electron localization effect of the Li bond beyond electrostatic interactions, which mainly dominate the ionic bond. Bond and electronic structure analyses further verify the difference between these two bonds. This work establishes principles to identify the Li bond and Li ionic bond, which contribute to Li chemistry and related applications, such as Li batteries.

INTRODUCTION

Lithium (Li) chemistry has become a significant branch of modern chemistry and has bred many momentous applications, including the Li battery, Li grease, Li medication, and nuclear reactions (Li deuteride).[1] As a milestone in the history of Li chemistry, the Li bond was proposed in 1959 by Shigorin and was considered as an analog of the hydrogen (H) bond due to the notable similarity between Li and H elements.[2–4] Despite similarities, the metallic nature of Li can afford the Li bond considerable ionicity, which is different from the H bond with a partial covalent bond nature (Table S1).[5,6] This gives rise to the mystery of the Li bond, especially that the principle of differentiating it from the conventional Li ionic bond (hereinafter referred to as ionic bond) is not yet established and remains a huge challenge. Meanwhile, the Li bond attracts great interest due to the increasingly important role of Li-related technologies currently.

Li battery, which is one of the most prevalent applications of the Li element, provides an arena for the fulfillment of the Li bond. The introduction of the Li bond into Li battery studies dates back to the 2010s.[7–16] A Li bond can form between a Li center and electron-donating atoms belonging to electrolyte species or electrode surfaces in batteries. Zhang and co-authors conducted a comprehensive study on such a bond in Li–sulfur batteries, and the Li bond was suggested as a dipole-dipole interaction in this case.[17] However, the nature of the Li bond and its distinctions from the ionic bond are still ambiguous to afford a deep insight into this chemical bonding.

All rights are reserved, including those for text and data mining, AI training, and similar technologies.

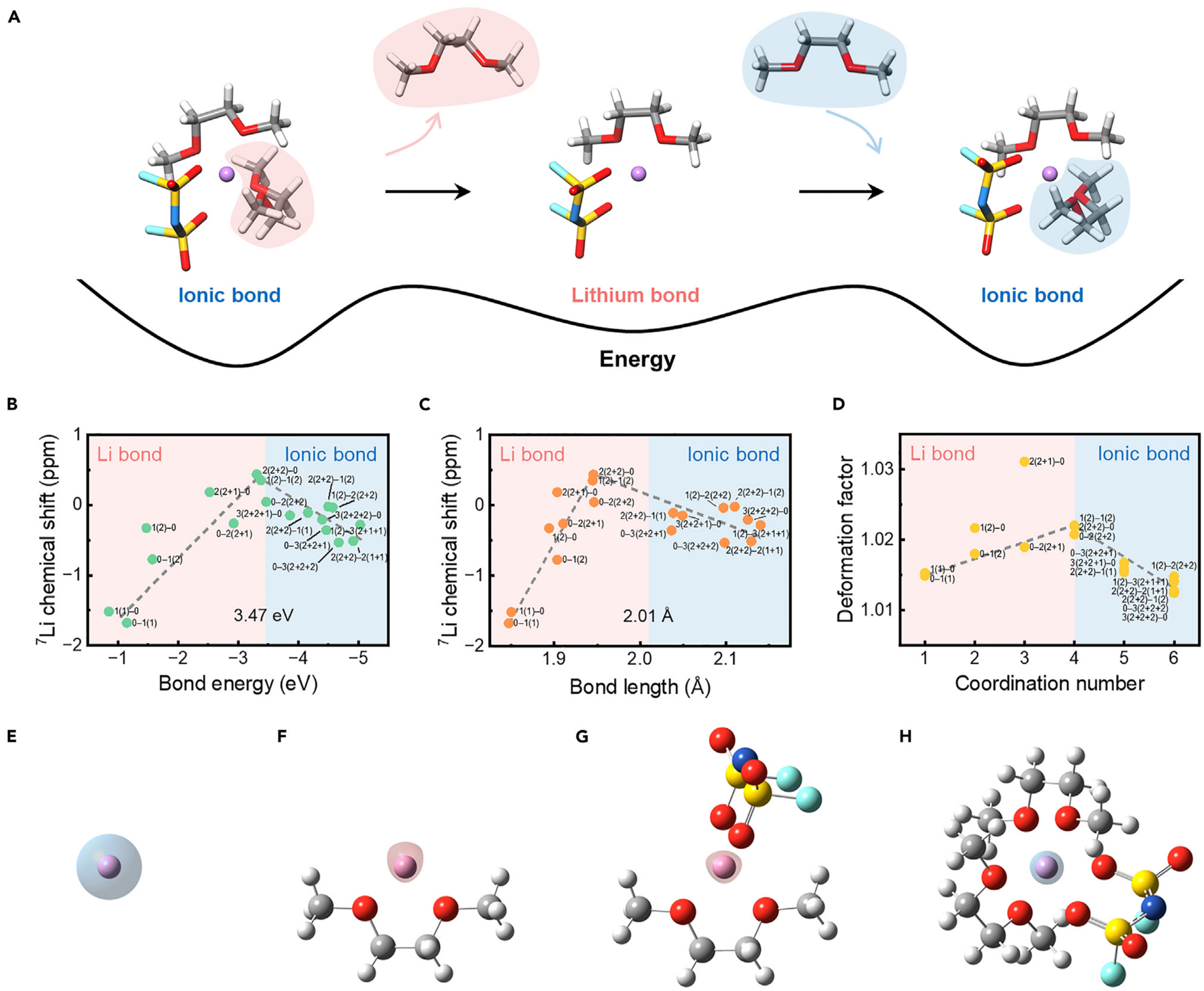

Figure 1. Lithium bond and lithium ionic bond analysis based on the interactions between Li and O atoms of 1,2-dimethoxyethane and bis(fluorosulfonyl)imide anion

(A) Schematic of the ionic and Li bond transition.

(B) Change of ^{7}Li chemical shift with bond energy between Li and O atoms of bonding species, i.e., DME or FSI^-. The labels M and N indicate the respective number of DME (M) and FSI^- (N), and the numbers in brackets represent mono- (1) or bi-dentate (2) of each bonding molecule.

(C) Change of ^{7}Li chemical shift with the bond length between Li and O atoms of coordinated species.

(D) Deformation factor of the electron localized function (ELF) around Li at an isovalue of 0.5.

(E–H) Visualized ELF in (E) Li^+, (F) Li^+-DME, (G) Li^+-DME–FSI^-, and (H) Li^+-DME_2–FSI^- structures. Atomic color: H, white; Li, violet; C, gray; N, blue; O, red; F, cyan; and S, yellow.

In this contribution, the principles of identifying the Li bond are established by a comprehensive investigation of Li-centered clusters in battery electrolytes, including the analyses of the ^{7}Li nuclear magnetic resonance (NMR) spectroscopy, bond energy, bond length, and electronic structure. The Li atom interacts with oxygen (O) atoms from electrolyte solvents or anions, forming the Li bond and ionic bond at low and high coordination number (CN) conditions, respectively (Figure 1A). The strengthening of the Li bond induces a downfield shift of the ^{7}Li NMR signal, which is consistent with the case of the H bond. The spatial deformation of the Li electronic structure caused by O atoms proves to be responsible for such a trend, indicating the electron localization effect of the Li bond. For the ionic bond, the ^{7}Li peak shifts reversely due to the domination of electrostatic interactions. Notably, anions produce a stronger shielding effect compared with neutral molecules, giving rise to the overall upfield shift of the NMR peak with growing interactions between Li and anions. Our work reveals the fundamental difference between the Li bond and ionic bond: the former embodies a more significant electron localization feature than the latter. This sheds light on the distinctive properties of the Li bond and ionic bond and promotes the development of Li chemistry.

RESULTS

Strong electron-donating atoms such as nitrogen, O, and fluorine usually serve as the H bond acceptor, likewise for the Li bond. Considering the much more frequent interactions observed between Li and O than those between Li and the other two elements in Li battery electrolytes, 1,2-dimethoxyethane (DME) and bis(fluorosulfonyl)imide anion (FSI^-) interacting with Li by their O atoms are selected as representative bonding species. Models of one Li-ion coordinating with a total of 1 to 6 atoms from either DME or FSI^- are constructed since the large radius and metallic nature of Li allow it to bond at most 6 atoms (Figure S1). Also inspired by the characterization of the H bond, ^7Li NMR spectroscopy is adopted to probe the Li bond and ionic bond.[18]

The bond energy of Li and O atoms gradually rises when CN increases from 1 to 6, regardless of bonding molecules (Figure S2). However, the ^7Li chemical shifts in NMR exhibit a volcano trend with both the bond energy and CN (Figure 1B). The chemical shifts of ^7Li shift downfield at the initial increase of CN from 1 to 4, along with the growing bond energy. The less shielded ^7Li nucleus as the bond becomes stronger resembles the characteristic of the H bond.[19,20] The ^7Li signal subsequently shows an upfield shift with the increase of CN from 4 to 6 and the bond energy. A similar volcano relationship can be observed wherein the average Li–O bond length takes the place of the bond energy (Figure 1C). Specifically, the chemical shifts of ^7Li demonstrate a downfield shift followed by an upfield shift as the bond length increases. It should be noted that a larger bond energy corresponds to a longer bond length. Li can bind with more than 1 atom, and the NMR spectroscopy characterizes the effects caused by all the species around the Li center. In this case, the "bond" here, which considers all Li–O bonds to accord with the NMR situation, and the traditional bond between only two atoms have a twist on the meaning. The longer the average bond length, the weaker the average bond energy, and the larger the overall bond energy due to more binding species (Figure S3).

It is generally acknowledged that the chemical shifts in NMR spectroscopy are primarily determined by the electronic environment around the observed nucleus, especially the electron density. The atomic charge based on the natural bond orbital analysis (NBO charge) is used to probe this quantity of the Li nucleus (Figure S4). The NBO charge of Li becomes negative monotonously with increasing CN, suggesting a growing electron density around Li ought to induce a stronger shielding effect. This, however, is not consistent with the deshielding of Li at CN of 1 to 4. Besides the electron density, the NMR shielding tensors depend on the kinetic energy density under the framework of density functional theory.[21,22] A deformation factor (ϕ) of the electron localization function (ELF) around Li, which can afford the kinetic energy density information with the elimination of effects caused by electron density, is therefore defined (see details in experimental procedures).[23] It is worth noting that ELF is also determined by electron spins, and the shielding on the nucleus is highly dependent on electron spins as evidenced by distinct ^{17}O chemical shifts of singlet and triplet O_2 (Figure S5). Therefore, the ELF and its deformation are in close relation to the electronic environment around Li to rationalize its chemical shift change. The ϕ of ELF of the bare Li-ion is almost unity (1.005) corresponding to a "perfect" baseline of kinetic energy density and electron spins, whereas a larger deviation of ϕ from this value signifies a more prominent variation of the electronic environment aroused by bonding species (Figures 1D–1H). As CN increases from 1 to 4, the ϕ increases from around 1.015 to over 1.020, and that in the Li–$DME_{2(2+1)}$ structure even exceeds 1.031 (Figures 1D, 1F, and 1G). The significant change of ELF delivers a weaker shielding effect compared with the perfect distribution, and hence the Li nucleus is less shielded despite the more negative charge and higher energy density. The values of ϕ then fall back to be close to unity at CN of 5 (around 1.016) and 6 (around 1.013), where the electron density prevails over the change of kinetic energy density and electron spins, resulting in a strong shielding effect and the upfield shift of the ^7Li chemical shift (Figures 1D and 1H).

Considering the two distinct trends of the ^7Li chemical shifts, the Li–O interactions are classified as the Li bond and ionic bond in the deshielding and shielding regions, respectively. A tipping point with a CN of 4 is observed to differentiate these two bonds. On the one hand, the Li nucleus in the ionic bond is shielded by electronegative O atoms due to dominating electrostatic interactions, while the Li bond delivers an electron localization effect as evidenced by the change of kinetic energy density of Li due to bonding atoms. This effect outperforms the shielding effects from electronegative O atoms and produces a deshielding effect on Li. On the other hand, the bond energy and length of the ionic bond in the Li_2O crystal, which are 3.47 eV and 2.01 Å, respectively, precisely separate the Li bond and ionic bond.[24] This further validates the boundary of these two bond types.

Moreover, O atoms from the neutral DME and anionic FSI^- influence the Li–O bond properties diversely. The chemical shifts of ^7Li in structures with more O atoms from FSI^- are located upfield in comparison to those with more DME atoms, indicating that the anion can induce a stronger shielding effect on the Li nucleus than the neutral molecule can (Figure 2A). Nevertheless, the NBO charge analysis shows DME molecules contribute more greatly to the negative charge of Li than FSI^- (Figure 2B). The smaller ϕ of ELF caused by FSI^- than DME rationalizes this, as a smaller ϕ corresponds to a stronger shielding effect (Figure 2C). Hence, attention should be paid to the electron distribution instead of merely focusing on the charge on Li atoms.

Beyond the microscopic characterization of the Li bond and ionic bond based on the Li^+-DME/FSI^- interaction models, the Li bonding chemistry is explored at the electrolyte level. The 1.05, 2.01, and 4.02 M LiFSI in DME electrolytes (hereinafter referred to as LC, MC, and HC, respectively) are considered (Figures 3A–3C).[25] The FSI^- anion has a higher probability of bonding Li with a rising LiFSI concentration (Figures 3D–3F). Simultaneously, solvent molecules are less involved in the coordination with Li as indicated by the decreasing proportion of solvation shells with more than one DME molecule (Figure S6). In the LC electrolyte, the number of anions bonding each Li-ion ranges from 0 to 4, and corresponding structures account for 2.0%, 23.1%, 46.5%, 25.3%, and 3.1%, respectively, in all existing structures (Figure 3D). The structure distribution of the MC electrolyte is similar to that of the LC one, but the proportion of Li–FSI^-_x (x = 3 and 4) grows by

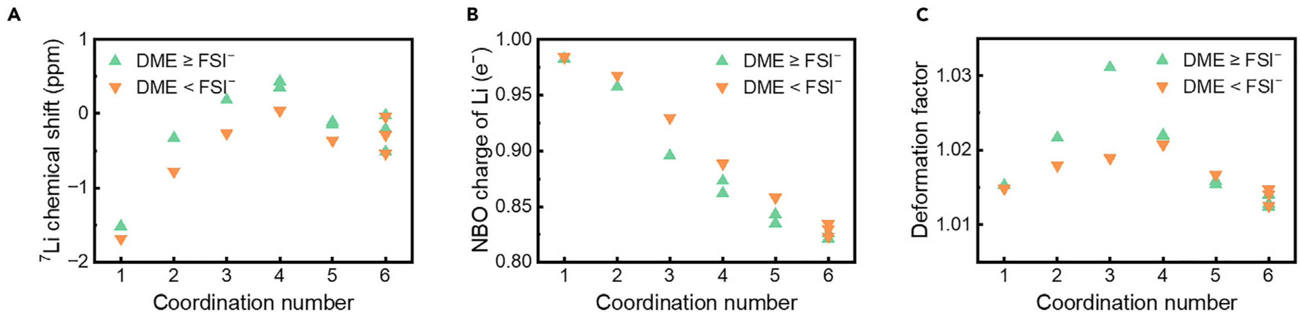

Figure 2. Diverse effects of the neutral DME and anionic FSI^- on the Li–O bond properties

(A) ^{7}Li chemical shift of Li in different bonding structures with different coordination numbers. DME $\geq$ FSI^- corresponds to structures where the coordination number contributed by DME is larger than or equal to that by FSI^-, while DME < FSI^- is the opposite.

(B) NBO charge of Li in different bonding structures.

(C) Deformation factor of the ELF around Li at an isovalue of 0.5 in different bonding structures.

12.1% (Figure 3E). The structures of Li–$FSI^-{}_5$ emerge in the HC electrolyte at a percentage of 9.7, and the proportion of Li interacting with more than 2 FSI^- keeps increasing to 63.4% relative to the LC and MC electrolytes (Figure 3F).

The NMR signal of each Li in the electrolyte will contribute to the ultimate signal of this system. Consequently, the ^{7}Li chemical shifts in different bonding configurations are all characterized (Figure S7, see details in experimental procedures). The ^{7}Li chemical shifts deliver a general downfield trend with the growing bond energy, which conforms with the feature of the ionic bond. This trend can also be inferred from the CN of Li. Those Li, whose CN is larger than 4, occupy nearly 100% of all Li in electrolytes regardless of the salt concentration (Figure S8). Only around 2.4% Li bonds are observed in the HC electrolyte while negligible Li bonds exist in the LC and MC electrolytes. However, the Li bond is involved in the solvation and desolvation process of the Li-ion, which therefore probably plays a significant role in regulating the Li-ion transport (Figure S9). All

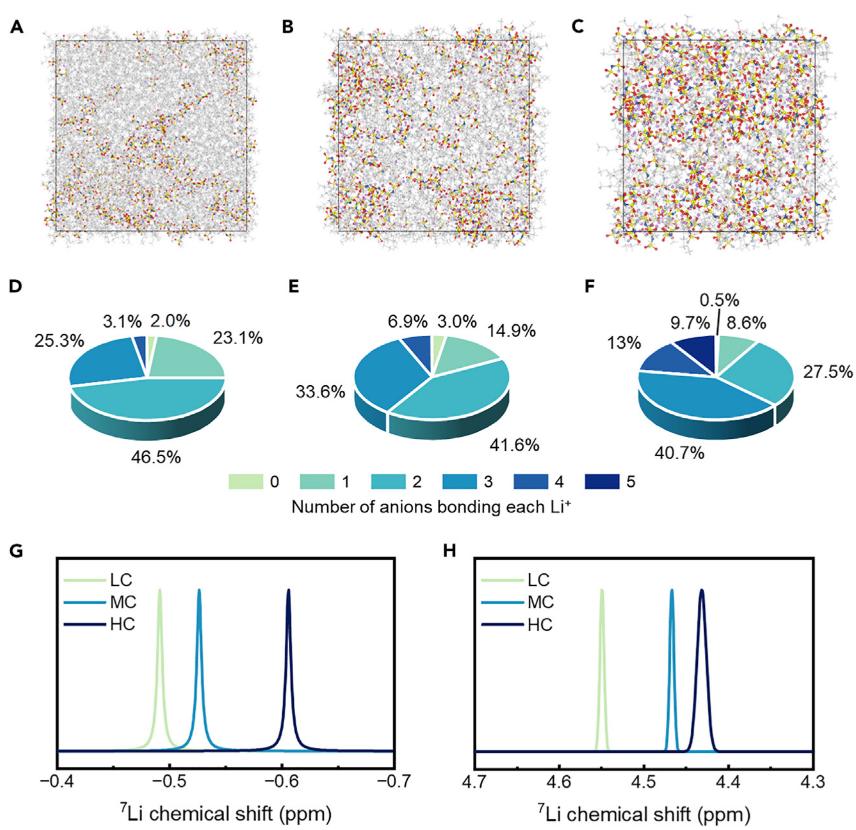

Figure 3. Li bonding analysis based on low-, moderate-, and high-salt-concentration DME/LiFSI electrolytes

Three electrolytes are denoted as LC, MC, and HC, respectively.

(A–C) Snapshots of molecular dynamics (MD) simulations on (A) LC, (B) MC, and (C) HC DME/LiFSI electrolytes.

(D–F) Bonding structure distributions of (D) LC, (E) MC, and (F) HC DME/LiFSI electrolytes. 0 to 5 represent the number of anions bonding each Li.

(G and H) (G) Theoretical and (H) experimental NMR spectra of LC, MC, and HC DME/LiFSI electrolytes.

chemical shifts are then averaged to produce the final result of each electrolyte. Following the FSI^- bonding Li to a greater extent in the sequence of LC, MC, and HC electrolytes, the ^7Li NMR shifts upfield from -0.49 to -0.53 and -0.61 ppm given that FSI^- anions induce a stronger shielding effect than DME molecules do as mentioned previously (Figures 2A and 3G). This theoretically predicted trend of NMR chemical shifts is further validated by the experimental measurement. In detail, experimental chemical shifts of ^7Li in LC, MC, and HC electrolytes are 4.55, 4.47, and 4.43 ppm, respectively. More anions participate in the solvation shell of Li^+ with the increasing salt concentration, and the central Li^+ gets more shielded to show a consistent variation trend with theoretical calculations. These results guarantee the reliability of our theoretical insight into the bonding of Li and its dependence on actual structures of electrolytes (Figure 3H).

DISCUSSION

The Li bond and ionic bond are characterized in detail in our work by the bonding between Li and O atoms of routine molecules in Li battery electrolytes. These two bond types can be distinguished from each other according to distinct responses of the Li nucleus in the NMR spectroscopy. In detail, ^7Li chemical shifts shift downfield and upfield in the Li bond and ionic bond, respectively, with the increasing bond energy, and the Li bond behaves resembling the H bond. Especially, the noteworthy deformation of the ELF around the Li atom induced by bonding atoms corresponds to a strong electron localization effect of the Li bond as opposed to the ionic bond controlled by electrostatic interactions. The nature of the Li bond is therefore unveiled, affording a fruitful insight into the Li bonding chemistry. In addition, Li and its bonding atoms will experience dynamic evolutions in electrolytes with fluctuating bond features. The Li bond provides a metastable state with comparable energy with that of the ionic bond, probably favoring the faster transport of Li in electrolytes than in Li-containing solids.[26–28] The significance and applications of the Li bond deserve further exploration. Studies on the bonding between Li and other atoms such as nitrogen and fluorine are also needed to conclude a universal principle of the Li bond and fulfill the Li chemistry.

EXPERIMENTAL PROCEDURES

Resource availability

Lead contact

Further information and requests for resources should be directed to and will be fulfilled by the lead contact, Qiang Zhang (zhang-qiang@mails.tsinghua.edu.cn).

Materials availability

This study did not generate new, unique reagents.

Data and code availability

The data that support the findings of this study are available within this article and its supplemental information. Additional data are available from the corresponding authors upon reasonable request.

^7Li and ^{17}O chemical shift

Both DME and FSI^- can interact with the Li atom by 1 or 2 O atom(s), and therefore possible bonding structures were constructed (Figure S1). These structures were optimized by Gaussian 16 using Lee-Yang-Parr correlation functional (B3LYP) at a basis set of 6–311++G(d,p) with the solvation model based on solute electron density (SMD) implemented with DME parameters (dielectric constant = 7.2, solvent radius = 4.19 Å) considered.[29–31] NMR shielding tensors of ^7Li in optimized structures were obtained at the same calculation level. The NMR shielding tensor of Li in Li^+–$(H_2O)_3$ was selected as the reference, which is also commonly used as the reference in experimental NMR characterizations. Therefore, ^7Li chemical shift equals the shielding tensor of Li in Li^+–$(H_2O)_3$ minusing that of Li in different bonding structures.

Bond energy

The Li bonding structures were optimized, and their energies were calculated first at the level mentioned above. The Li nucleus was then deleted from each structure to calculate the energy of species bonded to Li. The bond energy between the Li nucleus and its bonding species was defined as follows:

$$\textit{Bond energy} = E_{\mathrm{Li-DME_x-FSI^-{}_y}} - E_{\mathrm{Li}} - E_{\mathrm{DME_x-FSI^-{}_y}} \qquad \text{(Equation 1)}$$

where $E_{\mathrm{Li-DME_x-FSI^-{}_y}}$, E_{Li}, and $E_{\mathrm{DME_x-FSI^-{}_y}}$ (x = 0, 1, 2, and 3; y = 0, 1, 2, and 3) represent the total energy of the Li–DME and/or FSI^- bonding structures, Li nucleus, and DME and/or FSI^-, respectively.

Bond length

The lengths of all Li–O bonds in an optimized Li bonding structure were measured and then averaged to produce the bond length of the corresponding structure.

Deformation factor

The ELFs of Li in optimized Li bonding structures were analyzed by Multiwfn (Ver. 3.8dev).[32] ϕ was defined as follows:

$$\phi = \frac{A_{\mathrm{Li}}}{A_{\mathrm{Sphere}}} \qquad \text{(Equation 2)}$$

where A_{Li} denotes the surface area of ELF around the Li nucleus at an isovalue of 0.5 and A_{Sphere} the surface area of a sphere with the same volume as ELF.

MD simulation

Molecular dynamics (MD) simulations were conducted using the large scale atomic/molecular massively parallel simulator (LAMMPS) code (ver. 29 Sep 2021).[33] Three electrolyte models containing 200 LiFSI pairing with 1640, 760, and 280 DME molecules were constructed, respectively, corresponding to the LC, MC, and HC electrolytes. Parameters of DME were adopted from the optimized potentials for liquid simulations-all atom (OPLS-AA) force field except for using the advanced restrained electrostatic potential (RESP2) atomic partial charges obtained based on electrostatic potential (ESP) charges using Multiwfn (ver. 3.8dev).[32,34–36] Parameters of Li^+ and FSI^- were from Jensen et al. and Lopes et al., respectively.[37,38] The initial atomic coordinates were generated with PACKMOL (ver. 20.010), and the MD snapshots were visualized with VESTA (ver. 3.5.7).[39,40]

Firstly, all electrolyte models were equilibrated in an isothermal-isobaric (constant NPT) ensemble using the Parrinello-Rahman barostat for 2.0 ns to maintain a temperature of 298 K and a pressure of 1 atm. After that, the electrolytes were heated from 298 to 450 K within 0.5 ns, maintained at 450 K for 1.0 ns, and then cooled from 450 to 298 K within 0.5 ns, followed by equilibration at 298 K for another 4 ns. A 7 ns production run was finally conducted in the canonical (constant NVT) ensemble under the Nose–Hoover thermostat. The final 5 ns were sampled to analyze the Li bonding structures. All Li bonding structures in the very last 1 fs of each simulation were extracted to calculate the ^7Li chemical shifts without structure optimization and to produce the NMR results of LC, MC, and HC DME/LiFSI electrolytes.

Experimental NMR spectroscopy

LiFSI was dissolved in DME to produce 1.0, 2.0, and 4.0 M DME/LiFSI electrolytes, corresponding to the LC, MC, and HC electrolytes, respectively. The experimental ^7Li NMR spectra were recorded at 155.5 MHz using a JNM-ECZ400S system at room temperature. For each system, 0.5 mL prepared electrolyte solution was injected into a 5 mm NMR tube, and the test was conducted by scanning from −10 to 10 ppm each time and repeated 16 times. A 1.0 M sample of LiCl in H_2O was used as the reference (0 ppm).

SUPPLEMENTAL INFORMATION

Supplemental information can be found online at https://doi.org/10.1016/j.chempr.2024.07.016.

ACKNOWLEDGMENTS

This work was supported by the National Natural Science Foundation of China (T2322015, 22393900, 22393903, and 22109086), the National Key Research and Development Program (2021YFB2500300), and the Beijing Municipal Natural Science Foundation (Z200011). The authors acknowledged the support from the Tsinghua National Laboratory for Information Science and Technology for theoretical simulations.

AUTHOR CONTRIBUTIONS

N.Y., X.C., and Q.Z. conceived the idea for the project. N.Y., Y.-C.G., L.Y., Y.-B.G., and W.-L.L. conducted the quantum chemistry calculations and MD simulations. S.-Y.S. carried out the NMR experiments. All the authors discussed the results, analyzed the data, and drafted the manuscript.

DECLARATION OF INTERESTS

The authors declare no competing interests.

Received: April 2, 2024
Revised: June 7, 2024
Accepted: July 16, 2024
Published: August 20, 2024

REFERENCES

1. Sapse, A.-M., and Schleyer, P.v.R. (1995). Lithium Chemistry: A Theoretical and Experimental Overview, First Edition (John Wiley & Sons, Inc.).
2. Shigorin, D.N. (1959). Infra-red absorption spectra study of H-bonding and of metal-element bonding. Spectrochim. Acta *14*, 198–212. https://doi.org/10.1016/0371-1951(59)80229-0.
3. Kollman, P.A., Liebman, J.F., and Allen, L.C. (1970). Lithium bond. J. Am. Chem. Soc. *92*, 1142–1150. https://doi.org/10.1021/ja00708a007.
4. Ault, B.S., and Pimentel, G.C. (1975). Matrix isolation infrared studies of lithium bonding. J. Phys. Chem. *79*, 621–626. https://doi.org/10.1021/j100573a015.
5. Pauling, L. (1960). The Nature of the Chemical Bond, Third Edition (Cornell University Press).
6. Dereka, B., Yu, Q., Lewis, N.H.C., Carpenter, W.B., Bowman, J.M., and Tokmakoff, A. (2021). Crossover from hydrogen to chemical bonding. Science *371*, 160–164. https://doi.org/10.1126/science.abe1951.
7. Park, K., Cho, J.H., Jang, J.-H., Yu, B.-C., De La Hoz, A.T., Miller, K.M., Ellison, C.J., and Goodenough, J.B. (2015). Trapping lithium polysulfides of a Li–S battery by forming lithium bonds in a polymer matrix. Energy Environ. Sci. *8*, 2389–2395. https://doi.org/10.1039/C5EE01809A.
8. Liao, K.M., Mao, P., Li, N., Han, M., Yi, J., He, P., Sun, Y., and Zhou, H.S. (2016). Stabilization of polysulfides via lithium bonds for Li–S batteries. J. Mater. Chem. A *4*, 5406–5409. https://doi.org/10.1039/C6TA00054A.
9. Li, G., Lei, W., Luo, D., Deng, Y., Deng, Z., Wang, D., Yu, A., and Chen, Z. (2018). Stringed "tube on cube" nanohybrids as compact cathode matrix for high-loading and lean-electrolyte lithium–sulfur batteries. Energy Environ. Sci. *11*, 2372–2381. https://doi.org/10.1039/C8EE01377B.
10. Tu, S., Chen, X., Zhao, X., Cheng, M., Xiong, P., He, Y., Zhang, Q., and Xu, Y. (2018). A polysulfide-immobilizing polymer retards the shuttling of polysulfide intermediates in lithium–sulfur batteries. Adv. Mater. *30*, e1804581. https://doi.org/10.1002/adma.201804581.
11. Cai, W., Li, G., Luo, D., Xiao, G., Zhu, S., Zhao, Y., Chen, Z., Zhu, Y., and Qian, Y. (2018). The dual-play of 3D conductive scaffold embedded with Co, N codoped hollow polyhedra toward high-performance Li–S full cell. Adv. Energy Mater. *8*, 1802561. https://doi.org/10.1002/aenm.201802561.
12. Maihom, T., Kaewruang, S., Phattharasupakun, N., Chiochan, P., Limtrakul, J., and Sawangphruk, M. (2018). Lithium bond impact on lithium polysulfide adsorption with functionalized carbon fiber paper interlayers for lithium–sulfur batteries. J. Phys. Chem. C *122*, 7033–7040. https://doi.org/10.1021/acs.jpcc.7b09392.
13. Mortemard de Boisse, B., Nishimura, S.-i., Watanabe, E., Lander, L., Tsuchimoto, A., Kikkawa, J., Kobayashi, E., Asakura, D., Okubo, M., and Yamada, A. (2018). Highly reversible oxygen-redox chemistry at 4.1 V in $Na_{4/7-x}[\square_{1/7}Mn_{6/7}]O_2$ (□: Mn vacancy). Adv. Energy Mater. *8*, 1800409. https://doi.org/10.1002/aenm.201800409.
14. Wang, C., Wu, J.B., Zhao, X.X., Wang, L.L., and Yin, Z.X. (2021). Lithium bond-enhanced capacity of dipyridyl polysulfides for LSBs. ACS Appl. Energy Mater. *4*, 3495–3501. https://doi.org/10.1021/acsaem.0c03236.
15. Yang, L., Huang, Y.X., Tufail, M.K., Wang, X.F., and Yang, W. (2022). An unprecedented fireproof, anion-immobilized composite electrolyte obtained via solidifying carbonate electrolyte for safe and high-power solid-state lithium-ion batteries. Small *18*, e2202060. https://doi.org/10.1002/smll.202202060.
16. Tian, Z., Hou, L., Feng, D., Jiao, Y., and Wu, P. (2023). Modulating the coordination environment of lithium bonds for high performance polymer electrolyte batteries. ACS Nano *17*, 3786–3796. https://doi.org/10.1021/acsnano.2c11734.
17. Hou, T.-Z., Xu, W.-T., Chen, X., Peng, H.-J., Huang, J.-Q., and Zhang, Q. (2017). Lithium bond chemistry in lithium–sulfur batteries. Angew. Chem. Int. Ed. Engl. *56*, 8178–8182. https://doi.org/10.1002/anie.201704324.
18. Cordier, F., Rogowski, M., Grzesiek, S., and Bax, A. (1999). Observation of through-hydrogen-bond $^{2h}J_{hc'}$ in a perdeuterated protein. J. Magn. Reson. *140*, 510–512. https://doi.org/10.1006/jmre.1999.1899.
19. Wagner, G., Pardi, A., and Wuethrich, K. (1983). Hydrogen bond length and proton NMR chemical shifts in proteins. J. Am. Chem. Soc. *105*, 5948–5949. https://doi.org/10.1021/ja00356a056.
20. Arnold, W.D., and Oldfield, E. (2000). The chemical nature of hydrogen bonding in proteins via NMR: J-couplings, chemical shifts, and AIM theory. J. Am. Chem. Soc. *122*, 12835–12841. https://doi.org/10.1021/ja0025705.
21. Maximoff, S.N., and Scuseria, G.E. (2004). Nuclear magnetic resonance shielding tensors calculated with kinetic energy density-dependent exchange-correlation functionals. Chem. Phys. Lett. *390*, 408–412. https://doi.org/10.1016/j.cplett.2004.04.049.
22. Franzke, Y.J., and Holzer, C. (2022). Impact of the current density on paramagnetic NMR properties. J. Chem. Phys. *157*, 031102. https://doi.org/10.1063/5.0103898.
23. Savin, A., Jepsen, O., Flad, J., Andersen, O.K., Preuss, H., and von Schnering, H.G. (1992). Electron localization in solid-state structures of the elements: The diamond structure. Angew. Chem. Int. Ed. Engl. *31*, 187–188. https://doi.org/10.1002/anie.199201871.
24. Rumble, J.R. (2022). CRC Handbook of Chemistry and Physics, 103rd Edition (CRC Press).
25. Qian, J., Henderson, W.A., Xu, W., Bhattacharya, P., Engelhard, M., Borodin, O., and Zhang, J.G. (2015). High rate and stable cycling of lithium metal anode. Nat. Commun. *6*, 6362. https://doi.org/10.1038/ncomms7362.
26. Yamada, Y., Wang, J., Ko, S., Watanabe, E., and Yamada, A. (2019). Advances and issues in developing salt-concentrated battery electrolytes. Nat. Energy *4*, 269–280. https://doi.org/10.1038/s41560-019-0336-z.

27. Lorger, S., Usiskin, R., and Maier, J. (2019). Transport and charge carrier chemistry in lithium oxide. J. Electrochem. Soc. *166*, A2215–A2220. https://doi.org/10.1149/2.1121910jes.

28. Shi, S., Qi, Y., Li, H., and Hector, L.G., Jr. (2013). Defect thermodynamics and diffusion mechanisms in Li_2CO_3 and implications for the solid electrolyte interphase in Li-ion batteries. J. Phys. Chem. C *117*, 8579–8593. https://doi.org/10.1021/jp310591u.

29. Frisch, M.J., Trucks, G.W., Schlegel, H.B., Scuseria, G.E., Robb, M.A., Cheeseman, J.R., Scalmani, G., Barone, V., Petersson, G.A., Nakatsuji, H., et al. (2016). Gaussian 16, Revision A.03 (Gaussian Inc.).

30. Becke, A.D. (1993). Density-functional thermochemistry. III. The role of exact exchange. J. Chem. Phys. *98*, 5648–5652. https://doi.org/10.1063/1.464913.

31. Marenich, A.V., Cramer, C.J., and Truhlar, D.G. (2009). Universal solvation model based on solute electron density and on a continuum model of the solvent defined by the bulk dielectric constant and atomic surface tensions. J. Phys. Chem. B *113*, 6378–6396. https://doi.org/10.1021/jp810292n.

32. Lu, T., and Chen, F.-W. (2012). Multiwfn: A multifunctional wavefunction analyzer. J. Comput. Chem. *33*, 580–592. https://doi.org/10.1002/jcc.22885.

33. Plimpton, S. (1995). Fast parallel algorithms for short-range molecular dynamics. J. Comput. Phys. *117*, 1–19. https://doi.org/10.1006/jcph.1995.1039.

34. Jorgensen, W.L., Maxwell, D.S., and Tirado-Rives, J. (1996). Development and testing of the OPLS all-atom force field on conformational energetics and properties of organic liquids. J. Am. Chem. Soc. *118*, 11225–11236. https://doi.org/10.1021/ja9621760.

35. Dodda, L.S., Cabeza de Vaca, I.C., Tirado-Rives, J., and Jorgensen, W.L. (2017). LigParGen web server: An automatic OPLS-AA parameter generator for organic ligands. Nucleic Acids Res. *45*, W331–W336. https://doi.org/10.1093/nar/gkx312.

36. Schauperl, M., Nerenberg, P.S., Jang, H., Wang, L.P., Bayly, C.I., Mobley, D.L., and Gilson, M.K. (2020). Non-bonded force field model with advanced restrained electrostatic potential charges (RESP2). Commun. Chem. *3*, 44. https://doi.org/10.1038/s42004-020-0291-4.

37. Jensen, K.P., and Jorgensen, W.L. (2006). Halide, ammonium, and alkali metal ion parameters for modeling aqueous solutions. J. Chem. Theory Comput. *2*, 1499–1509. https://doi.org/10.1021/ct600252r.

38. Canongia Lopes, J.N., Shimizu, K., Pádua, A.A.H., Umebayashi, Y., Fukuda, S., Fujii, K., and Ishiguro, S.-i. (2008). Potential energy landscape of bis(fluorosulfonyl)amide. J. Phys. Chem. B *112*, 9449–9455. https://doi.org/10.1021/jp803309c.

39. Martínez, L., Andrade, R., Birgin, E.G., and Martínez, J.M. (2009). PACKMOL: A package for building initial configurations for molecular dynamics simulations. J. Comput. Chem. *30*, 2157–2164. https://doi.org/10.1002/jcc.21224.

40. Momma, K., and Izumi, F. (2011). VESTA 3 for three-dimensional visualization of crystal, volumetric and morphology data. J. Appl. Crystallogr. *44*, 1272–1276. https://doi.org/10.1107/S0021889811038970.